Article

Growth of First Generation Dendrons on SiO: Controlling Chemisorption of Transition Metal Coordination Complexes

Manish Sharma, Abhishek Dube, and James R. Engstrom

J. Am. Chem. Soc., **2007**, 129 (48), 15022-15033 • DOI: 10.1021/ja0752944

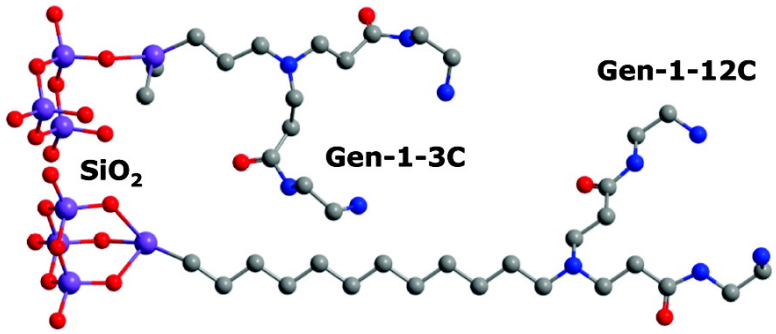

J|A|C|S
ARTICLES
Published on Web 11/13/2007

Growth of First Generation Dendrons on SiO_2: Controlling Chemisorption of Transition Metal Coordination Complexes

Manish Sharma, Abhishek Dube, and James R. Engstrom*

Contribution from the School of Chemical and Biomolecular Engineering, Cornell University, Ithaca, New York 14853

Received July 16, 2007; E-mail: jre7@cornell.edu

Abstract: We have investigated the growth of first generation branched polyamidoamine dendrons on silicon dioxide as a way to tailor and control the subsequent chemisorption of transition metal coordination complexes. Beginning with straight-chain alkyl, amine-terminated self-assembled monolayers as anchors, we find that the efficiency of the dendritic branching step depends on the length of the anchor, it being nearly perfect on a 12-carbon chain anchor. The reaction of these layers, both the anchor layers and the first generation dendrons, with $Ta[N(CH_3)_2]_5$ and $Ti[N(CH_3)_2]_4$ have been examined in ultrahigh vacuum using X-ray photoelectron spectroscopy. We find that the saturation coverage increases with the density of terminal $-NH_2$ groups; thus, the branching step has effectively amplified the chemisorptive capacity of the surface. Concerning the spatial extent of reaction we find that it depends on the thickness and structure of the organic layer. The thinnest layer cannot prevent penetration of the metal complex to the organic/SiO_2 interface, where it can react with residual $-OH$, whereas, on the longer straight chain anchor, reaction occurs exclusively at the terminal $-NH_2$ group. On the branched dendrons, the situation is more complex, and reaction occurs not only with the terminal $-NH_2$ group but also likely with functional groups, such as $-NH-(C=O)-$, on the backbone of the branched dendron.

1. Introduction

Interfaces play an important and sometimes dominant role in determining the performance characteristics of many modern solid-state devices.[1] To date, inorganic−inorganic interfaces such as $Si-SiO_2$ have been most prevalent in semiconductor technologies. There is increasing interest, however, in the incorporation of organic molecules as active components in semiconductor devices. Self-assembly is a popular and effective method to form what might be termed as organic-on-inorganic interfaces.[2−4] In order to completely realize the promise of organic molecules in such devices, methods to form *inorganic-on-organic* interfaces must also be developed.

One technology where inorganic-on-organic interfaces have potential application is for barrier and seed layers in interconnect structures. Currently, considerable research is directed at replacing SiO_2 as the interlayer dielectric (ILD) with materials having dielectric constants much less than 4, the so-called "low-κ dielectrics".[5] Various materials have been proposed, and it is very likely that materials possessing significant porosity will eventually be required. In order to prevent diffusion of the interconnect metal (Cu) atoms into the porous dielectric, it must be sealed by depositing an ultrathin film of, say, TiN [6,7] or TaN.[8,9] In principle, the deposition of these barrier layers, which must be conformal over high aspect ratio features, can be achieved by atomic layer deposition (ALD).[10,11] This has proved to be problematic. For example, nucleation of the barrier layer on porous dielectrics is difficult often due to their molecular composition, and by definition, their void spaces provide no sites for thin film nucleation. It is here that an appropriately designed interfacial organic layer may provide a solution. Ideally, such a layer would maximize the surface density of potential nucleation sites, and the evolution of its structure would be intrinsically self-expanding and space filling.

Organic layers that possess a dendritic structure might fulfill the need for both filling space and providing nucleation sites. Polyamidoamine (PAMAM) dendrimers[12−14] are three-dimensional, highly ordered, tree-like branched macromolecules that

(1) Streetman, B. G.; Banerjee, S. *Solid State Electronic Devices*; Prentice Hall: 2000.
(2) Ulman, A. *An introduction to Ultrathin Organic Films: From Langmuir-Blodgett to self assembly*; Academic Press: 1991.
(3) Dubois, L. H.; Nuzzo, R. G. *Annu. Rev. Phys. Chem.* **1992**, *43*, 437−463.
(4) Ulman, A. *Chem. Rev.* **1996**, *96*, 1533−1554.
(5) Morgen, M.; Ryan, E. T.; Zhao, J.; Hu, C.; Cho, T.; Ho, P. S. *Annu. Rev. Mater. Sci.* **2000**, *30*, 645−680.
(6) Maisonobe, J. C.; Passemard, G.; Lacour, C.; Lecornec Motte, P.; Noel, P.; Torres, J. *Microelectron. Eng.* **2000**, *50*, 25−32.
(7) Satta, A.; Baklanov, M.; Richard, O.; Vantomme, A.; Bender, H.; Conard, T.; Maex, K.; Li, W. M.; Elers, K. E.; Haukka, S. *Microelectron. Eng.* **2002**, *60*, 59−69.
(8) Min, K. H.; Chun, K. C.; Kim, K. B. *J. Vac. Sci. Technol. B* **1996**, *14*, 3263−3269.
(9) Tsai, M. H.; Sun, S. C.; Chiu, H. T.; Tsai, C. E.; Chuang, S. H. *Appl. Phys. Lett.* **1995**, *67*, 1128−1130.
(10) Ritala, M.; Asikainen, T.; Leskela, M.; Jokinen, J.; Lappalainen, R.; Utriainen, M.; Niinisto, L.; Ristolainen, E. *Appl. Surf. Sci.* **1997**, *120*, 199−212.
(11) Kim, D. J.; Jung, Y. B.; Lee, M. B.; Lee, Y. H.; Lee, J. H.; Lee, J. H. *Thin Solid Films* **2000**, *372*, 276−283.
(12) Tomalia, D. A.; Baker, H.; Dewald, J.; Hall, M.; Kallos, G.; Martin, S.; Roeck, J.; Ryder, J.; Smith, P. *Polym. J.* **1985**, *17*, 117−132.
(13) Tomalia, D. A.; Baker, H.; Dewald, J.; Hall, M.; Kallos, G.; Martin, S.; Roeck, J.; Ryder, J.; Smith, P. *Macromolecules* **1986**, *19*, 2466−2468.
(14) Padias, A. B.; Hall, H. K.; Tomalia, D. A.; Mcconnell, J. R. *J. Org. Chem.* **1987**, *52*, 5305−5312.

10.1021/ja0752944 CCC: $37.00

can be synthesized in a highly controllable manner using a divergent[15] or a convergent method.[16] They possess reactive surface and/or terminal groups, and the density of these, as well as the degree of branching, increases with the number of times (i.e., "generations") the sequential growth process is repeated. Owing to their molecular structure,[17,18] dendrimers may find important applications in fields such as gene therapy,[19,20] drug delivery,[21,22] sensors,[23−25] catalysis, [26,27] and surface modification.[28] In many cases preformed solution synthesized dendrimers have been immobilized on solid substrates such as silica,[29] gold,[30] and mica.[31] In this approach the dendrimer is bound to the substrate by the surface/terminal groups, which may or may not involve covalent bonding. Alternatively, in some applications one may wish to initiate growth at the substrate surface and ensure covalent attachment. Indeed, solid-phase synthesis of dendrimers has been studied on high surface area substrates such as ultrafine silica and polymeric beads in colloidal solutions of these supports. The applications of solid supported dendrimers include enhancement of resin loading[32−36] with dendrimers acting as efficient DNA carriers; palladium-complexed dendrimers acting as recyclable catalysts for hydroesterification reactions[37] and dendrimer growth on carbon black for controlling its surface properties.[38]

Other approaches have been attempted concerning the growth of oligomeric and polymeric organic layers on surfaces. Using organomercaptan self-assembled monolayers (SAMs) as an anchor, hyperbranched polymer films consisting of branches of a random copolymer of poly(acrylic acid) and poly(acrylamide) have been grown on Au surfaces.[39] The thickness of these films increased nonlinearly with the number of discrete synthetic steps. There has also been work concerning the growth from surfaces of polymeric films that possess a linear backbone, such as alkyl polyamide[40] and nylon-66.[41] In these studies polymerization was achieved by exposing the surface in an alternating fashion to vapors of the monomers. Solution-phase chemistry, including click chemistry,[42] has also been used for the layer-by-layer growth of polymer films that possess linear carbon backbones.[43]

Once the polymeric thin film has been formed, whether it be dendritic, branched, or linear, in applications as we mentioned above one may wish to deposit an inorganic thin film on the organic layer. In terms of dendritic layers, there have been a few studies directed at examining the evaporative deposition of metal thin films (e.g., Au, Cu, Cr, Co) directly on the dendrimer.[44−47] In one study, the adhesion of Au to amine terminated polyamidoamine (PAMAM) dendrimers (bound to SiO_2) was found to be effective only for the eighth generation dendrimer.[44] In another study, Cr and Co films were deposited on a PAMAM layer adsorbed on SiO_2, and X-ray photoelectron spectroscopy (XPS) showed that the metal penetrates the dendrimer to form metal nitride in each case.[46] For the relatively unreactive metals, Au and Cu, XPS found evidence for the "disruption" of the dendrimer layer (penetration by the metal) but none for the formation of a nitride.[45] In general, studies of the deposition of metals on dendrimer layers by "physical" methods (e.g., evaporation, sputter deposition) found formation of a mixed/composite metal−dendrimer layer.

In the work reported here we have examined the formation of first generation polyamidoamine dendrons on SiO_2 surfaces that have been functionalized with self-assembled monolayers [$-(CH_2)_n-NH_2$, $n = 3, 12$]. After formation of the SAMs, a generation 1 layer is formed by subsequent reactions with methylacrylate and ethylenediamine. The organic layers (both generation 0, i.e., the SAM, and generation 1, the dendron) have been characterized using contact angle measurements, ellipsometry, and XPS. The choice of $-NH_2$ termination is not accidental. In previous work we have demonstrated that SAMs that possess terminal amine groups can react with transition metal coordination complexes via simple ligand exchange reactions.[48,49] Thus, these layers can act to seed further growth of a transition metal/transition metal nitride thin film.[50,51] As a consequence we have also characterized the reactivity of these layers toward two transition metal coordination complexes, tetrakis(dimethylamido)titanium, $Ti[N(CH_3)_2]_4$, and pentakis-

(15) Tomalia, D. A.; Durst, H. D. *Top. Curr. Chem.* **1993**, *165*, 193−313.
(16) Wooley, K. L.; Hawker, C. J.; Frechet, J. M. J. *J. Am. Chem. Soc.* **1991**, *113*, 4252−4261.
(17) Naylor, A. M.; Goddard, W. A.; Kiefer, G. E.; Tomalia, D. A. *J. Am. Chem. Soc.* **1989**, *111*, 2339−2341.
(18) Tomalia, D. A.; Naylor, A. M.; Goddard, W. A. *Angew. Chem., Int. Ed. Engl.* **1990**, *29*, 138−175.
(19) Ong, K. K.; Jenkins, A. L.; Cheng, R.; Tomalia, D. A.; Durst, H. D.; Jensen, J. L.; Emanuel, P. A.; Swim, C. R.; Yin, R. *Anal. Chim. Acta* **2001**, *444*, 143−148.
(20) Koping-Hoggard, M.; Varum, K. M.; Issa, M.; Danielsen, S.; Christensen, B. E.; Stokke, B. T.; Artursson, P. *Gene Ther.* **2004**, *11*, 1441−1452.
(21) Quintana, A.; Raczka, E.; Piehler, L.; Lee, I.; Myc, A.; Majoros, I.; Patri, A. K.; Thomas, T.; Mule, J.; Baker, J. R., Jr. *Pharm. Res.* **2002**, *19*, 1310−1316.
(22) Jang, W. D.; Kataoka, K. *J. Drug Delivery Sci. Technol.* **2005**, *15*, 19−30.
(23) Valerio, C.; Fillaut, J. L.; Ruiz, J.; Guittard, J.; Blais, J. C.; Astruc, D. *J. Am. Chem. Soc.* **1997**, *119*, 2588−2589.
(24) Albrecht, M.; Gossage, R. A.; Spek, A. L.; van Koten, G. *Chem. Commun. (Cambridge, U.K.)* **1998**, 1003−1004.
(25) Schlupp, M.; Weil, T.; Berresheim, A. J.; Wiesler, U. M.; Bargon, J.; Mullen, K. *Angew. Chem., Int. Ed.* **2001**, *40*, 4011−+.
(26) Scott, R. W. J.; Sivadinarayana, C.; Wilson, O. M.; Yan, Z.; Goodman, D. W.; Crooks, R. M. *J. Am. Chem. Soc.* **2005**, *127*, 1380−1381.
(27) Knapen, J. W. J.; Vandermade, A. W.; Dewilde, J. C.; Vanleeuwen, P. W. N. M.; Wijkens, P.; Grove, D. M.; Vankoten, G. *Nature* **1994**, *372*, 659−663.
(28) Zhang, X. Y.; Wilhelm, M.; Klein, J.; Pfaadt, M.; Meijer, E. W. *Langmuir* **2000**, *16*, 3884−3892.
(29) Knecht, M. R.; Sewell, S. L.; Wright, D. W. *Langmuir* **2005**, *21*, 2058−2061.
(30) Hierlemann, A.; Campbell, J. K.; Baker, L. A.; Crooks, R. M.; Ricco, A. J. *J. Am. Chem. Soc.* **1998**, *120*, 5323−5324.
(31) Hellmann, J.; Hamano, M.; Karthaus, O.; Ijiro, K.; Shimomura, M.; Irie, M. *Jpn. J. Appl. Phys. Part 2* **1998**, *37*, L816−L819.
(32) Fromont, C.; Bradley, M. *Chem. Commun.* **2000**, 283−284.
(33) Lebreton, S.; How, S. E.; Buchholz, M.; Yingyongnarongkul, B. E.; Bradley, M. *Tetrahedron* **2003**, *59*, 3945−3953.
(34) Dahan, A.; Weissberg, A.; Portnoy, M. *Chem. Commun.* **2003**, 1206−1207.
(35) Gebbink, R. J. M. K.; Kruithof, C. A.; Klink, G. P. M.; Koten, G. V. *Rev. Mol. Biotechnol.* **2002**, *90*, 183−193.
(36) Wells, N. J.; Basso, A.; Bradley, M. *Biopolymers* **1998**, *47*, 381−396.
(37) Reynhardt, J. P. K.; Alper, H. *J. Org. Chem.* **2003**, *68*, 8353−8360.
(38) Tsubokawa, N.; Satoh, T.; Murota, M.; Sato, S.; Shimizu, H. *Polym. Adv. Technol.* **2001**, *12*, 596−602.
(39) Zhou, Y.; Bruening, M. L.; Bergbreiter, D. E. M. C. R.; Wells, M. *J. Am. Chem. Soc.* **1996**, *118*, 3773−3774.
(40) Kubono, A.; Yuasa, N.; Shao, H. L.; Umemoto, S.; Okui, N. *Thin Solid Films* **1996**, *289*, 107−111.
(41) Shao, H. I.; Umemoto, S.; Kikutani, T.; Okui, N. *Polymer* **1997**, *38*, 459−462.
(42) Such, G. K.; Quinn, J. F.; Quinn, A.; Tjipto, E.; Caruso, F. *J. Am. Chem. Soc.* **2006**, *128*, 9318−9319.
(43) Kohli, P.; Blanchard, G. J. *Langmuir* **2000**, *16*, 4655−4661.
(44) Baker, L. A.; Zamborini, F. P.; Sun, L.; Crooks, R. M. *Anal. Chem.* **1999**, *71*, 4403−4406.
(45) Rar, A.; Zhou, J. N.; Liu, W. J.; Barnard, J. A.; Bennett, A.; Street, S. C. *Appl. Surf. Sci.* **2001**, *175*, 134−139.
(46) Curry, M.; Arrington, D.; Street, S. C.; Xu, F. T.; Barnard, J. A. *J. Vac. Sci. Technol. A* **2003**, *21*, 234−240.
(47) Street, S. C.; Rar, A.; Zhou, J. N.; Liu, W. J.; Barnard, J. A. *Chem. Mater.* **2001**, *13*, 3669−3677.
(48) Dube, A.; Chadeayne, A. R.; Sharma, M.; Wolczanski, P. T.; Engstrom, J. R. *J. Am. Chem. Soc.* **2005**, *127*, 14299−14309.
(49) Killampalli, A. S.; Ma, P. F.; Engstrom, J. R. *J. Am. Chem. Soc.* **2005**, *127*, 6300−6310.
(50) Dube, A.; Sharma, M.; Ma, P. F.; Engstrom, J. R. *Appl. Phys. Lett.* **2006**, *89*, 164108.
(51) Dube, A.; Sharma, M.; Ma, P. F.; Ercius, P. A.; Muller, D. A.; Engstrom, J. R. *J. Phys. Chem. C* **2007**, *111*, 11045−11058.

Scheme 1

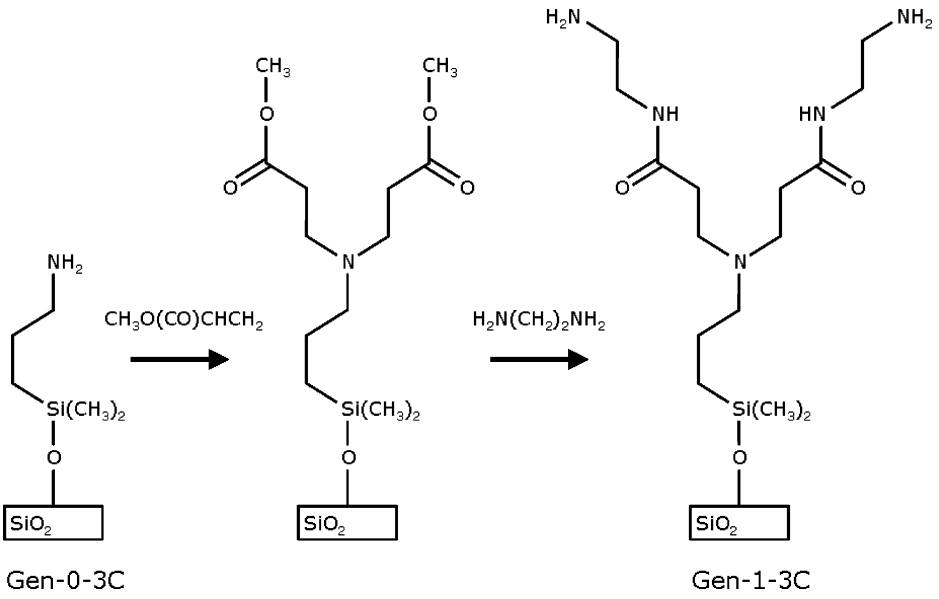

Table 1. Properties of the Organic Layers

organic layer	contact angle (deg) adv/rec	contact angle (deg) hysteresis	ellipsometric thickness (Å)	theoretical molecular length (Å)	calculated $-NH_2$ terminal density (cm^{-2})
		3C			
generation 0	$66.7 \pm 3.4/43.3 \pm 2.2$	23.4	5.7 ± 0.9	5.4	3.15×10^{14}
generation 1	$50.8 \pm 1.2/37.7 \pm 1.2$	13.1	11.2 ± 2.0	10.9	3.97×10^{14}
change	−15.9/-5.6	−10.3	+5.5	+5.5	
		12C			
generation 0	$64.0 \pm 0.9/45.3 \pm 1.9$	18.7	13.7 ± 3.3	16.9	2.63×10^{14}
generation 1	$41.3 \pm 1.0/28.0 \pm 0.9$	13.3	19.5 ± 1.7	21.6	5.01×10^{14}
change	−22.7/-17.3	−5.4	+5.8	+4.7	

(dimethylamido)tantalum, $Ta[N(CH_3)_2]_5$. In particular, using angle-resolved XPS, we will examine explicitly the tendency of the coordination complexes to engage in ligand exchange reactions with the terminal amine groups vs penetration of the organic layers and possibly reaction with the underlying SiO_2. We will also consider explicitly the change in reactivity of the layers as a function of generation, which will shed light on the ability of this approach to control the density of chemisorbed transition metal coordination complexes, which could profoundly affect thin film nucleation.

2. Experimental Procedures

Complete details concerning the experimental procedures employed here are in the Supporting Information, and we only give a brief summary here of the elements most essential to this study. In this work the first step involved the formation of two types of $-NH_2$ terminated self-assembled monolayers covalently bound to a chemically oxidized Si(100) wafer (referred to as "chemical oxide", *ca.* 20−25 Å thick). One of these involved silanization using 3-aminopropyldimethylethoxysilane, forming a $-NH_2$ terminated 3-carbon backbone alkyl SAM (referred to as Gen-0-3C). The other involved silanization using 11-cyanoundecyltrichlorosilane, which, after subsequent hydroboration, forms a $-NH_2$ terminated 12-carbon backbone alkyl SAM (referred to as Gen-0-12C). These Gen-0 SAMs served as the anchor from which generation 1 layers were formed by successive reaction with methyl acrylate (forming Gen-0.5) and ethylenediamine (forming Gen-1). This reaction strategy (*cf.* Scheme 1, only 3C is shown) is essentially the divergent type solvent phase synthesis used to make polyamidoamine (PAMAM) dendrimers.[12] The organic layers, at all generations, were examined using contact angle measurements, ellipsometry, and XPS, including angle resolved XPS. Both Gen-0 and Gen-1 layers were also exposed to the transition metal coordination complexes in a custom designed ultrahigh vacuum chamber,[52] which also served as the chamber where the studies using XPS were conducted.

3. Results and Discussion

3.1. Characterization of the Organic Layers. In Table 1 we report contact angles (advancing and receding), the thickness deduced from ellipsometry, the thickness predicted from the estimated molecular length (ACD/ChemSketch, Toronto, ON, Canada), and the calculated (from XPS) density of terminal $-NH_2$ groups for the organic layers considered here. The contact angles measured for the Gen-0 SAMs for both species (3C and 12C) are found to be in close agreement with those reported previously: namely 59.4°/47° [49] and 63°/42°[53] for Gen-0-12C (adv/rec) and 62.5°/38.7° for Gen-0-3C.[54] Also, the measured ellipsometric thicknesses are within 6 and 20% of the theoretical molecular length of the Gen-0-3C and Gen-0-12C anchors.

After treating the Gen-0 SAMs to produce the branched Gen-1 structures we observe changes in both the contact angles and the ellipsometric thicknesses, as may be seen in Table 1. For both anchors, we see a decrease in the contact angle in going from Gen-0 to Gen-1 (*ca.* −20° for the advancing angles). This

(52) Xia, L. Q.; Jones, M. E.; Maity, N.; Engstrom, J. R. *J. Vac. Sci. Technol. A* **1995**, *13*, 2651−2664.
(53) Balachander, N.; Sukenik, C. N. *Langmuir* **1990**, *6*, 1621−1627.
(54) Kanan, S. A.; Tze, W. T. Y.; Tripp, C. P. *Langmuir* **2002**, *18*, 6623−6627.

decrease may be attributed to an increase in the hydrophilic character of the surface due to an increase in the density of terminal $-NH_2$ groups. It is interesting to note that while we observe similar contact angles for both Gen-0 layers, a larger decrease in the contact angle is seen for the 12C anchor. This result would suggest that the degree of branching is more efficient for the longer starting anchor, perhaps due to steric reasons. Concerning the trend in the contact angle hysteresis, we see that for both anchors there is a decrease, whereas the decrease is largest for the 3C anchor. Hysteresis is most often associated with the perfection of the monolayer (less defects, smaller hysteresis[55]). Based solely on hysteresis, our results would suggest that the Gen-0-3C layer is the most defective and/or least homogeneous. However, following the Gen-1 synthesis step, both the 3C and 12C layers exhibit essentially the same hysteresis, suggesting similar homogeneity.

After carrying out the Gen-1 synthesis step a clear increase in the ellipsometric thickness is also seen for both the 3C and 12C layers. As may be seen in Table 1, the thickness of the layers increase by 5.5 and 5.8 Å for 3C and 12C, respectively. These increases are in *remarkable agreement* based on the expected changes in molecular length and further emphasize the efficiency of the branching step.

XP spectra have been obtained for all four layers considered in Table 1 (both anchors, both generations). First, a survey scan (0−1300 eV kinetic energy) was performed, and in all cases the spectra showed only the peaks corresponding to the presence of Si, C, O, and N. Second, detailed scans were acquired for the C(1s) and N(1s) peaks. Finally, angle resolved XP spectra were obtained for the C(1s) and Si(2p) regions.

In Figure 1 we display the C(1s) XP spectra for both (generation 0) anchors, 3C and 12C. A similar set of spectra for corresponding generation 1 layers are shown in Figure 2. First, a cursory inspection of Figures 1 and 2 reveals that the trend in the C(1s) peak intensity tracks that of the measured ellipsometric thickness: Gen-0-3C < Gen-1-3C < Gen-0-12C < Gen-1-12C. Second, the full widths at half-maximum for these features are larger than that expected for emission from a single oxidation state of C, and as may be seen, we have fit these features to multiple peaks. Multiple peaks are expected given the structure of these layers. For the two Gen-0 SAMs we expect contributions from C bound to Si ($R-CH_2-Si$) and from aliphatic ($R-CH_2-R$) and amino ($R-CH_2-NH_2$) carbons. One expects the former two to be described by a similar oxidation state, whereas a peak shift of 1.4 eV between aliphatic and amino (higher binding energy) carbons is expected.[56] For convenience, we will label the peak for aliphatic carbon (incl. those bound to Si) as C1 and that from the amino carbon as C2. As may be seen in Figure 1, both features are well fit to two peaks separated by 1.4 eV, and the ratio of areas, C2/C1, is found to be 0.35 for 3C and 0.32 for 12C. In comparison, the expected ratios of the number of amino to aliphatic carbon atoms for the two Gen-0 SAMs is 0.25 for 3C and 0.091 for 12C. These differences between expected and measured values are due mostly to photoelectron attenuation as the amino carbons will be the least attenuated if they reside at the SAM/vacuum interface as expected. Indeed the difference is smallest for the shorter SAM, where attenuation effects are also the smallest.

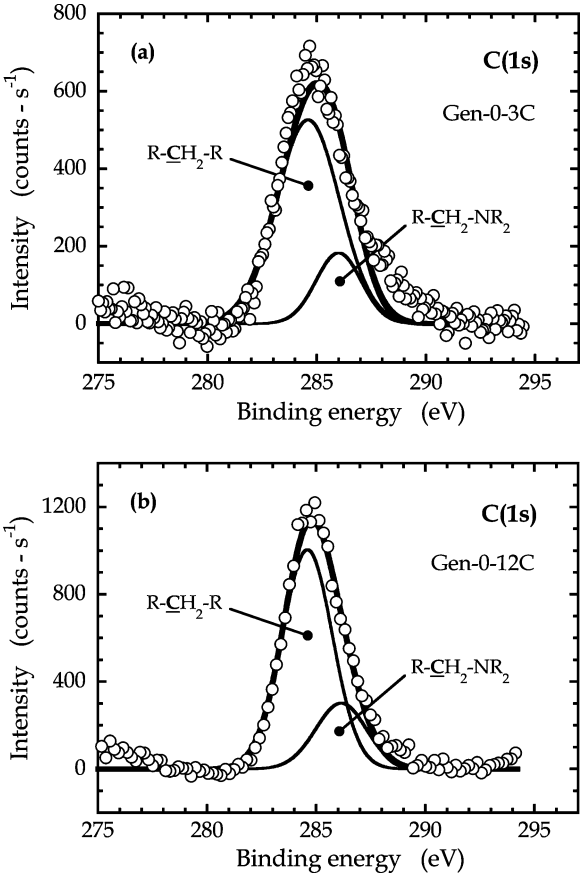

Figure 1. XP spectra of the C(1s) feature for Gen-0 SAMs: (a) 3C; and (b) 12C. The spectra have been fit to two peaks: the one at a binding energy of 284.6 eV corresponds to aliphatic carbons ($R-CH_2-R$), and the one at 286 eV, to amino carbon ($R-CH_2-NH_2$).

Moving on to the C(1s) XP spectra for the Gen-1 layers, in addition to the aliphatic and amino carbons, we now expect contributions also from the amidic carbons [$-C(=O)-NH-$]. Thus, the C(1s) spectra for the Gen-1-3C and -12C layers were fit to three peaks separated by binding energy shifts of 1.4 and 3.8 eV with respect to the aliphatic peak at 284.6 eV.[57, 58] We now label the peak at 3.8 eV higher binding energy as C3 (for the amidic carbon). As may be seen the C(1s) features in Figure 2 are fit well by these three peaks. From these fits, the ratio of the areas of the peaks for 3C are C2/C1 = 0.98 and C3/C1 = 0.24. Similarly, for Gen-1-12C, the integrated intensity ratios are C2/C1 = 0.72 and C3/C1 = 0.20. To summarize these results we have tabulated the predicted stoichiometry of the layers and that deduced from XPS, and these results appear in Table 2. As may be seen, there is *remarkably good agreement* between the values implicated from XPS and those predicted. Given the aforementioned attenuation effects, such agreement is not surprising for the shorter Gen-1-3C layer but perhaps unexpected for the thicker Gen-1-12C layer.

We now consider the N(1s) spectra for the four organic layers, and these spectra are displayed in Figure 3. In principle the N(1s) intensity should be a rather direct measure of the density of the two Gen-0 anchors. As may be seen, the intensity observed from the Gen-0-3C layer exceeds that from the Gen-

(55) Joanny, J. F.; Degennes, P. G. *J. Chem. Phys.* **1984**, *81*, 552−562.
(56) Kishi, K.; Ehara, Y. *Surf. Sci.* **1986**, *176*, 567−577.
(57) Demathieu, C.; Chehimi, M. M.; Lipskier, J. F.; Caminade, A. M.; Majoral, J. P. *Appl. Spectrosc.* **1999**, *53*, 1277−1281.
(58) Peeling, J.; Hruska, F. E.; Mckinnon, D. M.; Chauhan, M. S.; Mcintyre, N. S. *Can. J. Chem.* **1978**, *56*, 2405−2411.

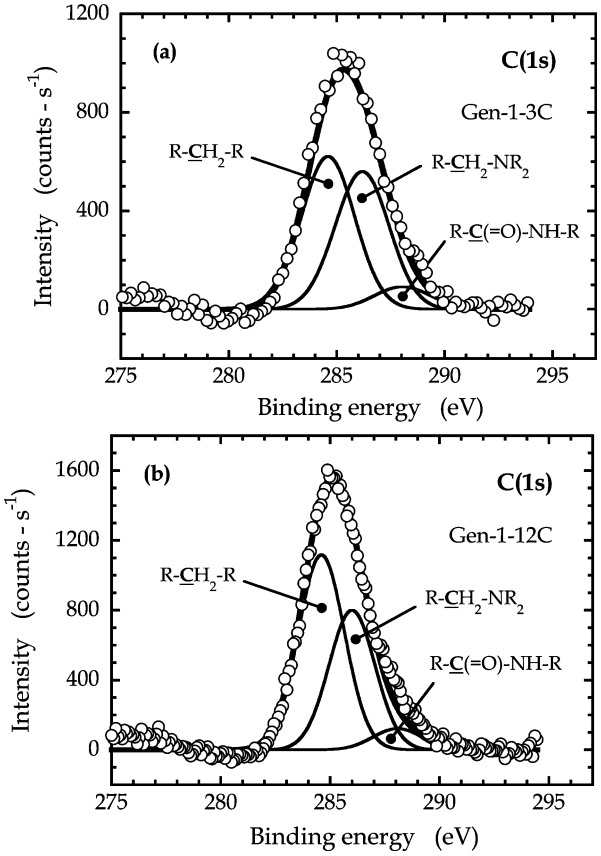

Figure 2. XP spectra of the C(1s) feature for Gen-1 layers: (a) 3C and (b) 12C. The spectra have been fit to three peaks: the one at a binding energy of 284.6 eV corresponds to aliphatic carbons (R−*C*H$_2$−R); the one at 286 eV, to amino carbons (R−*C*H$_2$−NH$_2$); and the one at 288.4, to amidic carbons (−*C*(=O)−NH−).

Table 2. Stoichiometry of Gen-1 Organic Layers

	Gen-1-3C		Gen-1-12C	
type of C	XPS	theoretical	XPS	theoretical
aliphatic	0.452	0.4	0.522	0.591
amino	0.441	0.467	0.374	0.318
amidic	0.106	0.133	0.104	0.091

0-12C, and the ratio of integrated intensities is 1.66. This suggests a higher (average) density for the Gen-0-3C monolayer. Also of interest is the relative change of the N(1s) feature following the branching step. We expect, of course, an increase in the intensity for this feature in both cases in going from Gen-0 to Gen-1. In the absence of attenuation effects the ratio N(Gen-1)-to-N(Gen-0) should be 5 if the branching step involves complete conversion of all terminal −NH$_2$ groups. For the 3C layer we see that the increase is modest, and the ratio of integrated intensities is 1.5. For the 12C layer, the increase is much more substantial and the ratio is 3.42. A number of factors could contribute to the observation of the N(Gen-1)-to-N(Gen-0) ratio being less than 5. First, attenuation effects clearly can play a role, as the Gen-1 synthesis step adds 5−6 Å of organic thin film, which will be denser than the Gen-0 layer when the Gen-1 step involves complete conversion. This would mostly affect the intensity from the branching N atom, and somewhat less from the amido N atom. Second, reactions might be incomplete at both (addition and condensation) stages of the synthesis.[12] There are many effects that might lead to incomplete

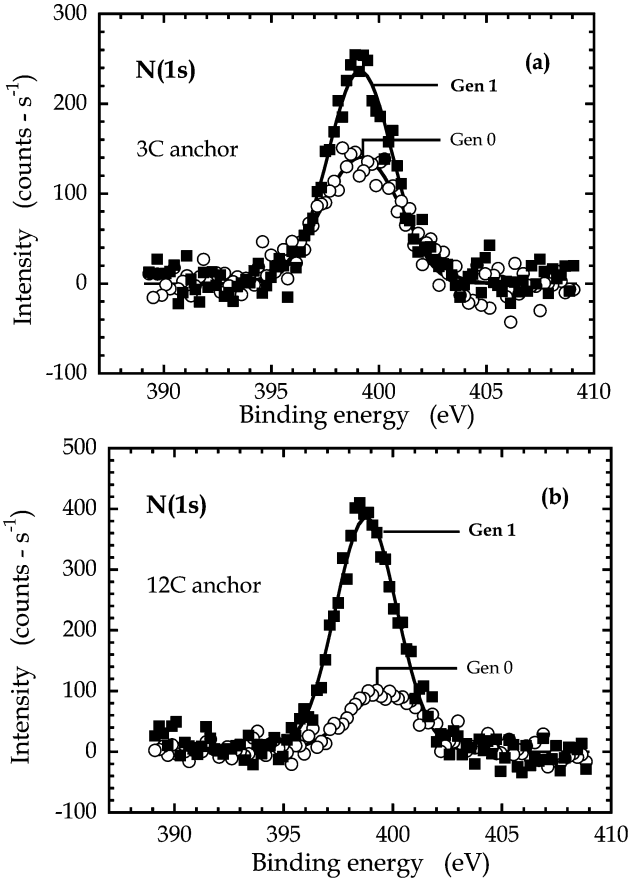

Figure 3. XP spectra of the N(1s) feature for both generations: (a) 3C and (b) 12C. Spectra have been fit to a single peak in each case. Empty symbols are for the Gen-0 anchors (○); filled are for the Gen-1 layers (■).

reactions, such as steric effects. In addition, competing reactions that do not follow Scheme 1 may also lead to a reduced amount of N added in the Gen-1 step.

Returning to our results for the C(1s) features, these spectra may also be used to estimate the absolute density of the Gen-0 SAMs and the absolute density that is added in the Gen-1 step. In the Supporting Information we provide complete details for this calculation, including the model used, how we make use of ARXPS data for the C(1s) feature, and how the density is calculated. The calculated densities are given in Table 1. Given the assumptions we have made here and the experimental uncertainties, we estimate the absolute accuracy of these values to be ±30%. For Gen-0 layers, we see that we estimate densities of 3.15×10^{14} cm^{-2} for 3C and 2.63×10^{14} cm^{-2} for 12C. Due to the unambiguous nature of assembly for these layers, these densities are also that for the terminal −NH$_2$ groups. The ratio of densities, Gen-0-3C/Gen-0-12C, is 1.2 from this analysis, which is in fair agreement with that implicated by the N(1s) spectra (1.66). In previous work, we found a density of $(2.38 \pm 0.17) \times 10^{14}$ cm^{-2} for 12C,[49] whereas a value of $(1.98 \pm 0.50) \times 10^{14}$ cm^{-2} has been reported for 3C.[59] For Gen-1 layers, we see that we estimate densities of 3.97×10^{14} cm^{-2} for 3C and 5.01×10^{14} cm^{-2} for 12C. If the amount of C and N added follows the stoichiometry expected for Gen-1, then these values are also representative of the density of the terminal −NH$_2$ groups. From these values we see that the ratio of terminal

(59) Moon, J. H.; Shin, J. W.; Kim, S. Y.; Park, J. W. *Langmuir* **1996**, *12*, 4621−4624.

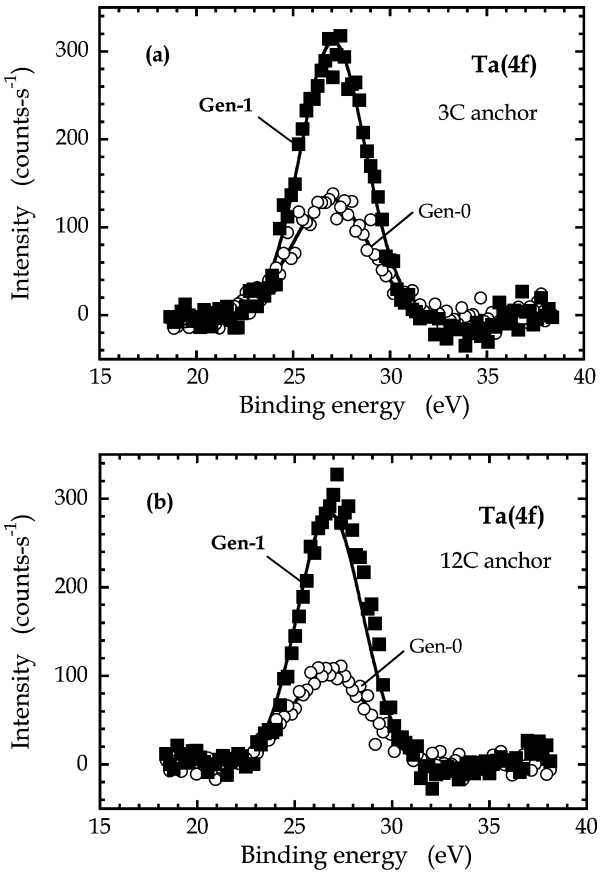

Figure 4. XP spectra of the Ta(4f) feature following saturation exposures of both the Gen-0 (○) and Gen-1 (■) layers of (a) 3C and (b) 12C to Ta-$[N(CH_3)_2]_5$ at $T_s = 25$ °C. In all cases, the spectra have been fit to a single peak [after removal of the contribution of the O(2s) feature; see Supporting Information].

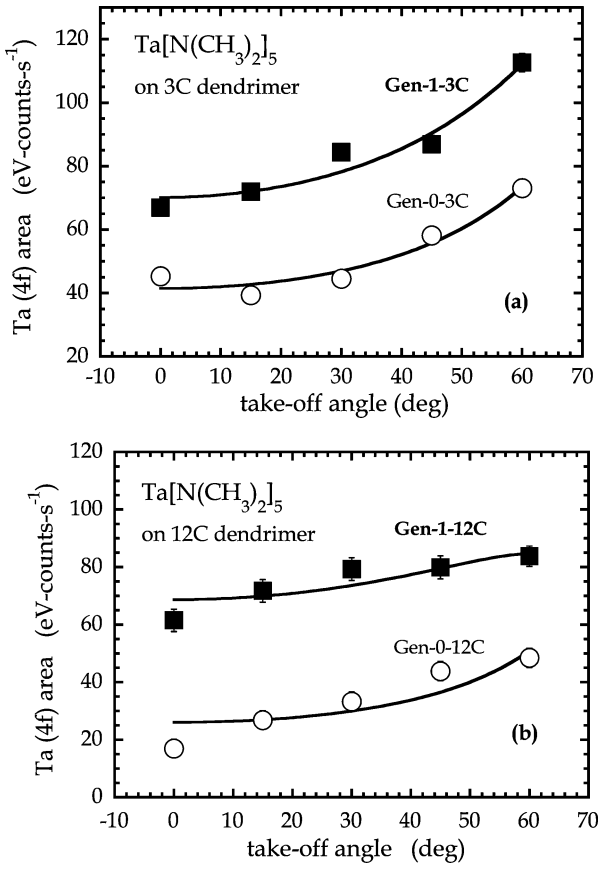

Figure 5. Peak area of the Ta(4f) region following saturation exposures of both the Gen-0 (○) and Gen-1 (■) layers of (a) 3C and (b) 12C to Ta-$[N(CH_3)_2]_5$ at $T_s = 25$ °C as a function of takeoff angle. The smooth curves are a fit to a model described in the text, which assumes that Ta is uniformly distributed at a depth d_M from the surface, and the values for d_M derived are shown in Table 3.

$-NH_2$ group densities for Gen-1 to Gen-0 is 1.26 for 3C and 1.90 for 12C. The observed deviation from the ideal value of 2 in each case might be attributed to incomplete reactions at Gen-0.5 and Gen-1 stages (reaction with methyl acrylate, and reaction with ethylene diamine) of the synthesis, more specifically retro Michael addition[60] and hydrolysis of the ester preventing its amidation. These nonidealities have been found to limit the yields of the dendrimer product also in solvent phase dendrimer synthesis.[12] Finally the incomplete conversion of the Gen-1 step implicated by this analysis, more so for the Gen-0-3C layer, is consistent with that suggested by the N(1s) spectra (*vide supra*).

A final set of analyses we have conducted on the substrates possessing the organic layers only are XPS and ARXPS of the Si(2p) region, and these results are given in the Supporting Information. Summarizing here, these results verify the conclusions made above, that an organic layer is formed in the generation 0 steps, which attenuates photoemission from the underlying SiO_2 substrate. In addition, the attenuation is increased as the Gen-1 layers are formed, and the attenuation is stronger for Gen-1 step on the 12 C anchor, indicating a more efficient conversion on the longer anchor.

3.2. Reaction of the Organic Layers with Ta and Ti Coordination Complexes. Having characterized the organic layers we now move on to an examination of their reactivity with two transition metal coordination complexes. We expect these complexes to react with the terminal $-NH_2$ groups (and possibly the $-NH-$ groups, *vide infra*) via ligand exchange reactions.[49] We consider first the reaction with Ta$[N(CH_3)_2]_5$. In this work the surfaces with the organic layers were exposed to the Ta complex at room temperature in the ultrahigh vacuum chamber. In situ XPS has been used to characterize the reactions between the Ta complex and the organic layers.

In order to compare the saturation coverages of Ta$[N(CH_3)_2]_5$ on the four interfacial organic layers, we have collected spectra in both the Ta(4f) and Ta(4d) regions. The coverage−exposure relationship for Ta$[N(CH_3)_2]_5$ on Gen-0 and Gen-1 12C indicated that the adsorption of the tantalum complex on these organic layers proceeded via first-order Langmuirian kinetics (details in the Supporting Information). The spectra in the Ta-(4f) region, while more intense, are complicated by the presence of an O(2s) peak, which we account for using the procedure outlined in the Supporting Information. In Figure 4 we plot the Ta(4f) spectra for both Gen-0 and Gen-1 on the (a) 3C and (b) 12C anchors. These spectra have been stripped of their O(2s) components. [A similar set of results for the Ta(4d) feature are given in the Supporting Information.] As may be seen from either figure, on both surfaces there is a significant increase in intensity going from Gen-0 to Gen-1. On the 3C layer the ratio of integrated intensities, $I_{Ta(4f),Gen-1-3C}/I_{Ta(4f),Gen-0-3C}$, is 2.03, while that on the 12C layer, $I_{Ta(4f),Gen-1-12C}/I_{Ta(4f),Gen-0-12C}$, is 2.41. Analysis of the Ta(4d) spectra give similar increases in the amount of chemisorbed Ta in going from Gen-0 to Gen-1,

(60) Kozlecki, T.; Samyn, C.; Alder, R. W.; Green, P. G. *J. Chem. Soc., Perkin Trans.* **2001**, *2*, 243−246.

Table 3. Properties of the Chemisorbed Layers

	penetration depth		density of metal (cm^{-2})	
	d_M/λ	d_M (Å)	uncorrected	corrected
		$Ta[N(CH_3)_2]_5$		
Gen-0-3C	0.12 ± 0.07	5.2 ± 3.1	$(1.19 \pm 0.30) \times 10^{14}$	$(1.39 \pm 0.37) \times 10^{14}$
Gen-1-3C	0.22 ± 0.06	5.7 ± 1.4	$(2.43 \pm 0.46) \times 10^{14}$	$(3.23 \pm 0.65) \times 10^{14}$
Gen-0-12C	0.02 ± 0.22	0.3 ± 3.1	$(0.96 \pm 0.25) \times 10^{14}$	$(0.99 \pm 0.38) \times 10^{14}$
Gen-1-12C	0.48 ± 0.08	8.5 ± 1.5	$(2.31 \pm 0.44) \times 10^{14}$	$(4.28 \pm 0.94) \times 10^{14}$
		$Ti[N(CH_3)_2]_4$		
Gen-0-3C	0.40 ± 0.06	14.7 ± 2.2	$(1.98 \pm 0.59) \times 10^{14}$	$(3.30 \pm 1.01) \times 10^{14}$
Gen-1-3C	0.26 ± 0.03	5.6 ± 0.6	$(2.49 \pm 0.72) \times 10^{14}$	$(3.47 \pm 1.01) \times 10^{14}$

namely a factor of 1.92 on the 3C anchor and 2.26 on the 12C anchor. This of course correlates with our estimates that the Gen-1 layers have a higher density of terminal $-NH_2$ groups. These results strongly support that the saturation coverage of the Ta complex is a strong function of the density of the terminal $-NH_2$ groups.

In order to quantify the amount of Ta chemisorbed on each surface we have obtained XP spectra from a polycrystalline Ta sheet, which we shall use as a reference standard. The area under this [Ta(4f)] peak is proportional to $\sigma_{Ta}N_{Ta}\lambda_{Ta}T(E_{Ta})$, where $\lambda_{Ta} = 19.4$ Å[61] and $N_{Ta} = 2.24 \times 10^{22}$ atoms cm^{-3}. [61] For photoemission from the Ta atoms in the chemisorbed layer we assume that they form a uniform thin film of thickness d_{Ta} and atomic density N'_{Ta}. If we further assume that the thickness of this layer is much less that the inelastic mean free path, i.e., $d_{Ta} \ll \lambda_{Ta}$, then the area under the peak for such an adlayer will then be proportional to $\sigma_{Ta}N'_{Ta}d_{Ta}T(E_{Ta})/\cos\theta$. With these assumptions, and the integrated peak areas for the reference Ta sample and for the organic layers exposed to $Ta[N(CH_3)_2]_5$, the quantity, $N'_{Ta}d_{Ta}$, which represents the Ta surface density, may be calculated directly. These values are given in Table 3 (labeled uncorrected) and range from 0.96×10^{14} to 2.43×10^{14} atoms cm^{-2}.

It is clear from the above discussion that $Ta[N(CH_3)_2]_5$ undergoes a gas-surface reaction with all four organic layers, and the amount of Ta deposited is best correlated with the density of terminal $-NH_2$ groups. An unresolved question concerns the spatial extent of this reaction, i.e., does the Ta complex react at the organic/vacuum interface, where the terminal $-NH_2$ groups reside, or might it penetrate the organic layer and react with other functional groups on the backbone, or perhaps residual $-OH$ at the organic/SiO_2 interface.[49] To address this issue we have acquired angle resolved XP spectra of the Ta(4f) feature. Again, these have been stripped of their O(2s) component. In Figure 5 we show the integrated intensities of the Ta(4f) features for both generations for 3C and 12C after saturation exposures to $Ta[N(CH_3)_2]_5$. First, at all takeoff angles the Ta(4f) intensity is greater for Gen-1 in both cases, consistent with the results presented in Figure 4. More importantly, it may be seen that, in all four cases, there is a clear increase in the integrated intensity with increasing takeoff angle. In general, for a species at the surface, the intensity should increase as the takeoff angle increases, whereas, for a species buried beneath the surface, the intensity will decrease at sufficiently large takeoff angles [*cf.* the results for Si(2p) in Figure S-3].

We have fit the data displayed in Figure 5 to a model that assumes the chemisorbed Ta is present in a two-dimensional plane at a distance d_{Ta} from the surface. In this case photoemission from such a film is given by $I(\theta) = (I_0/\cos\theta)\exp(-d_{Ta}/\lambda\cos\theta)$, where I_0 is the unattenuated emission achieved at normal takeoff angle. These fits are given by the smooth curves shown in Figure 5. These fits give values for the parameter d_{Ta}/λ. In order to estimate the (mean) penetration depth of the Ta layer, we need to estimate λ for the Ta(4f) photoelectrons. In this case we make use of the mean free path implicated by the ARXPS data for the C(1s) feature (found to depend on the layer), given in the Supporting Information, and the relation $\lambda_{Ta(4f)}/\lambda_{C(1s)} = \{E[Ta(4f)]/E[C(1s)]\}^{0.5}$, where E is the kinetic energy of the photoelectrons.[62] This procedure assumes that the $-N(CH_3)_2$ ligands retained by the chemisorbed Ta species do not alter the mean free path.

First, from the fits displayed in Figure 5 we find values for the parameter d_{Ta}/λ, and these values are given in Table 3. Making use of our estimates for the λ's, we also calculate d_{Ta}, and this is also given in Table 3. For 3C, we see that the distance the Ta is from the surface is essentially indistinguishable for the two generations. The size of the uncertainty for Gen-0-3C limits our conclusions as to the relative position of Ta in the organic layer. For the Gen-1-3C layer, the uncertainty is reduced and the implied depth is ~51% of the original thickness of the Gen-1-3C layer (11.2 Å), suggesting that Ta does not simply terminate the layer but forms a mixed adlayer. For Gen-0-12C, the data indicate that the Ta is bound to the terminal $-NH_2$ group and is at the surface, similar to previous observations for a Ti complex.[49] For Gen-1-12C, however, the implicated value for d_{Ta} is significant with respect to the measured ellipsometric thicknesses of 19.5 Å, representing 44% of this value. Thus, on both Gen-1 layers, some penetration and/or restructuring of the organic layer may have occurred.

We have also examined the reaction of $Ti[N(CH_3)_2]_4$ with these layers. In previous work[49] we have examined the reaction of this molecule with a Gen-0-12C layer. To summarize quickly, in this case we found that the Ti precursor reacted with the terminal $-NH_2$ group and that the reaction was limited to the SAM/vacuum interface. In particular, using the same model described above, $d_{Ti}/\lambda = 0.12 \pm 0.09$. On the other hand, for this same molecule, reaction on a surface terminated by a $-CH_3$ terminated C_{18} alkylsilane gave $d_{Ti}/\lambda = 0.86 \pm 0.19$, where essentially all observed reactivity could be assigned to the SAM/SiO_2 interface.

Here we have examined the reaction of $Ti[N(CH_3)_2]_4$ with Gen-0 and Gen-1-3C, and these results are shown in Figure 6.

(61) Mathieu, H. J.; Landolt, D. *Surf. Interface Anal.* **1984**, *6*, 82−89.

(62) *Practical Surface Analysis: Volume I, Auger and X-Ray Photoelectron Spectroscopy*, 2nd ed.; Seah, M. P., Briggs, D., Eds.; John Wiley and Sons: Chichester, U.K., 1990.

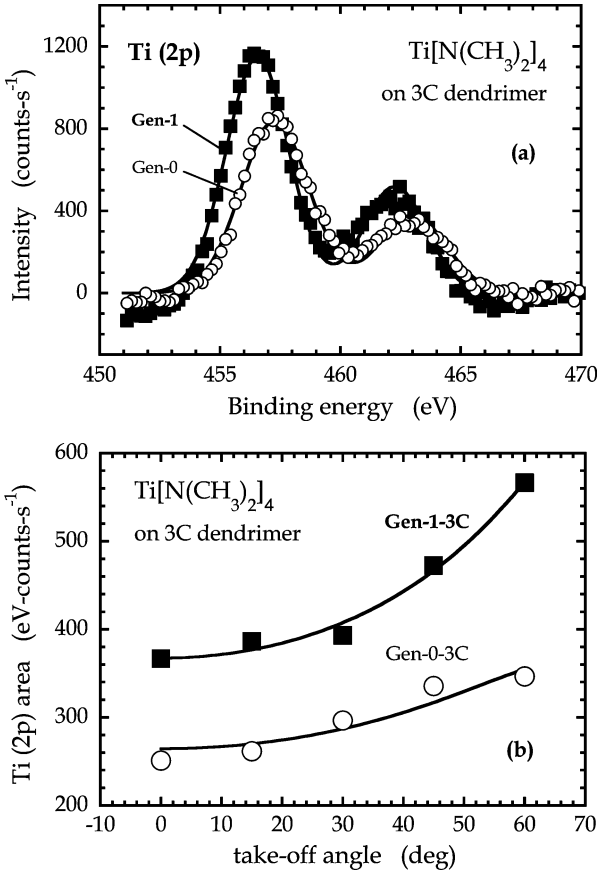

Figure 6. (a) XP spectra of the Ti(2p) feature following saturation exposures of both the Gen-0 (○) and Gen-1 (■) layers of the 3C anchor to $Ti[N(CH_3)_2]_4$ at $T_s = 25$ °C. The spectra have been fit to two peaks ($2p_{3/2}$, $2p_{1/2}$), corresponding to the split produced by the spin−orbit coupling. (b) Peak area of the Ti(2p) region of the same two layers as a function of takeoff angle. The smooth curves are a fit to a model described in the text, which assumes that Ti is uniformly distributed at a depth d_M from the surface, and the values for d_M derived are shown in Table 3.

The spectra for the Ti(2p) region are displayed in Figure 6a for saturation exposures of both 3C films to $Ti[N(CH_3)_2]_4$. Analogous to the results for Ta, the deposition of Ti is greater for the Gen-1 layer as compared to Gen-0. Making use of an approach essentially identical to that described above in connection with Figure 4, as well as elsewhere,[49] we can use these spectra to estimate the saturation coverage of $Ti[N(CH_3)_2]_4$ on these two surfaces. The values are given in Table 3. The values found for the 3C anchor can be compared to the value we found previously for $Ti[N(CH_3)_2]_4$ reacting with the Gen-0-12C layer, namely, $(2.47 \pm 0.19) \times 10^{14}$ atoms cm^{-2}.[49]

We have also used ARXPS to examine the spatial extent of reaction of $Ti[N(CH_3)_2]_4$ with both the Gen-0-3C and Gen-1-3C layers, and these results are shown in Figure 6b. As may be seen, there is an increase in the integrated peak areas for the Ti(2p) feature with an increase in takeoff angle for both generations. These data can be compared to similar data for $Ta[N(CH_3)_2]_5$ on these same two surfaces, *cf.* Figure 5a. We find values for d_{Ti}/λ (given in Table 3) that are comparable to, but larger than, those observed for the Ta species. Again, making use of estimates for the λ's for the Ti(2p) photoelectrons, we find values for the implicated depth of Ti from the surface. In the case of Gen-0-3C we find an unphysical value (depth larger than that of the layer itself), whereas for Gen-1-3C we find that d_{Ti} is ∼5.6 Å, or about 50% of the thickness of the original organic layer. This latter value is nearly identical to that observed for Ta (*vide supra*).

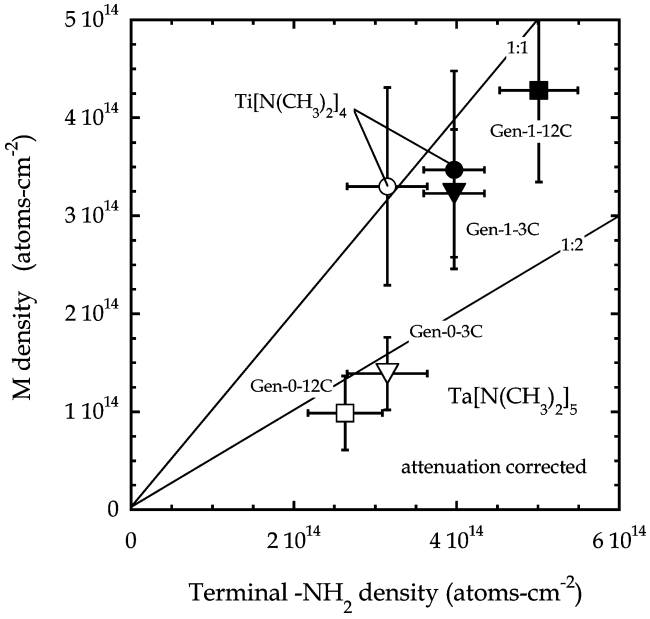

Figure 7. Saturation density of metal (Ta or Ti) in the adlayer as a function of the density of terminal $-NH_2$ groups in the organic layer. Open symbols represent results on the Gen-0 layers; filled represent results on the Gen-1 layers.

Next we will consider the stoichiometry of the adlayers that are formed. First as discussed above, due to the greater intensity of the C(1s) feature we have used it to estimate the density of terminal functional groups. In Figure 7 we plot the saturation density of the transition metal coordination complexes (corrected values) vs the (expected) density of terminal functional groups. Here, for the density of the metal, we have compensated for the attenuation of the photoelectrons emanating from the transition metal using the d/λ values found from ARXPS. (A similar plot using the uncorrected values for the density of metals is given in the Supporting Information.) As may be seen in the figure, there is a strong correlation between the density of the terminal functional groups and the saturation density of the metals. In terms of the number of functional groups that appear to have reacted with the transition metal coordination complexes via ligand exchange reactions, the ratio $-R-NH_2$/M, we find that for Ta on the Gen-0 layers it is between 2.3 ± 0.7 and 2.7 ± 1.1, whereas on the Gen-1 layers it is approximately 1.2 ± 0.3 for both anchors. For the Ti complex on the 3C layers: values of 0.95 ± 0.33 (Gen-0) and 1.15 ± 0.35 (Gen-1) are implicated. For the sake of argument, if we take the number for Ta on the Gen-0 layers as 2 for both cases, it is very comparable to results we have found previously for the reaction of $Ti[N(CH_3)_2]_4$ with Gen-0-12C[49] and for the reaction of this same molecule with oligo(phenylene-ethynylene) SAMs possessing an isopropyl termination.[48] Also, it suggests two possible scenarios: only one-half of the total terminal $-NH_2$ groups in the Gen-0 layers have reacted with the Ta metal complexes or each complex has reacted with two $-NH_2$ groups. Finally, these results, particularly those for the Ta complex, imply a superlinear dependence (a power law fit to the data would give an exponent > 1) of the uptake of metal complexes as a function of the density of terminal functional groups.

To conclude our discussion of the stoichiometry of the

Table 4. Stoichiometry, N/Metal, of Chemisorbed Adlayers at Saturation Exposures

	$Ta[N(CH_3)_2]_5$			$Ti[N(CH_3)_2]_4$
organic layer	Ta(4f)	Ta(4d)	Ta, mean	Ti(2p)
Gen-0-3C	5.32 ± 0.35	5.44 ± 0.52	5.38 ± 0.63	2.44 ± 0.20
Gen-1-3C	3.26 ± 0.15	3.46 ± 0.21	3.36 ± 0.26	1.64 ± 0.09
Gen-0-12C	3.35 ± 0.35	4.23 ± 0.65	3.79 ± 0.74	
Gen-1-12C	3.85 ± 0.19	4.86 ± 0.36	4.35 ± 0.40	

adlayers, we can also, using data from XPS, calculate the N/Ta (Ti) ratio. There are of course four possible contributors to the N signal: that from the unreacted $-N(CH_3)_2$ ligands and that due to the terminal $-NH_2$, backbone $-NH-$, and branching $-N<$ groups in the dendrons. The interpretation is therefore complicated. A very large N/Ta ratio, nevertheless, would indicate minimal ligand loss, whereas a smaller one would indicate increased ligand loss, perhaps even due to species such as residual $-OH(a)$ located at the organic/SiO_2 interface. Our results are shown in Table 4 for the reaction of both $Ta[N(CH_3)_2]_5$ (all layers) and $Ti[N(CH_3)_2]_4$ (just 3C layers). For the Ta complex we find that the ratio lies between about 3.3 and 5.4, whereas for the Ti complex it is clearly smaller, between about 1.6 and 2.4. To interpret these, we must account for the (terminal organic functional group)/M ratio, or OFG/M, and also the contributions of the backbone and branching N atoms for the Gen-1 layers. First, we start with the Gen-0 layers. The OFG/M for the Ta on Gen-0 layers lie between 2.3 and 2.7, as indicated above. If we define n to be this ratio there are two limits for the N/M ratio if only ligand exchange reactions occur. If the complex undergoes a single reaction, this leaves $n - 1$ OFGs unreacted per metal complex, and a N/M ratio of $n + 4$. In the other limit, all OFGs participate and the N/M ratio is constant at 5. Thus, for Ta on Gen-0-3C ($n \approx 2.3-2.6$) we expect $5 \leq N/M \leq 6.3-6.6$. The calculated value of 5.4 is most consistent with multiple ligand exchange reactions per complex. For Gen-0-12C, however, the value of 3.8 can only be explained by additional reactions. Such reactions that can reduce the N/Ta ratio include (i) ligand exchange reactions with residual $-OH$ at the organic layer/SiO_2 interface and (ii) ligand loss involving a hydrogen transfer from the amido linkage ($-NH-Ta$), eliminating $HN(CH_3)_2$, and forming an imido linkage ($-N=Ta$). Concerning the latter, the limit on these would be presumably 2 (setting a lower limit for N/Ta of 3), whereas steric factors may come into play concerning the former. As the ARXPS results indicate the Ta complex is at the surface, formation of imido linkages seems more likely.

Moving to the results for Ta on the Gen-1 layers, we see that N/Ta is $\sim 3.4-4.4$. Somewhat curiously, the value for Gen-1-3C is smaller than that for Gen-0-3C. Expectations for these Gen-1 layers are difficult to predict, as backbone $-NH-$ and possibly other groups [the $-NH(C=O)$ group as a whole] may contribute. First the OFG/M values for Ta are $n \approx 1.2-1.6$ on Gen-1-3C and $1.2-2.2$ on Gen-1-12C. If we count one backbone $-NH-$ and one-half branching $-N<$ per terminal $-NH_2$ OFG, then for single ligand exchange reactions with the terminal group the lower limit for N/Ta becomes $5 + 1.5n$, and the upper limit, $4 + 2.5n$. Clearly the calculated values for N/Ta suggest that additional reactions, as discussed above, occur on these layers. In addition to these two discussed above, reaction with the backbone $-NH-$ also comes into play.

Examination of the Ta(4d) spectra shown in the Supporting Information may shed some light on these issues, such as reactions with residual $-OH$ vs forming imido linkages. We note that the binding energies for the Ta($4d_{5/2}$) on the two Gen-1 layers and the Gen-0-12C layer are similar, namely 230.74 ± 0.02 (Gen-1-3C), 230.36 ± 0.02 (Gen-1-12C), and 230.65 ± 0.05 (Gen-0-12C), while that observed on Gen-0-3C is at 231.64 ± 0.05. The binding energy difference between Gen-0-3C and Gen-1-3C is $+0.90$ eV, a result that is consistent with more extensive reaction of $Ta[N(CH_3)_2]_5$ with residual $-OH$ for the thinner Gen-0-3C layer. For the 12C layers, however, we observe a much smaller difference between Gen-0-12C and Gen-1-12C layers of $+0.29$ eV, implying a more similar chemical environment for the Ta chemisorbed layer, and little reaction with residual $-OH$ in either case.

Finally we consider the results for $Ti[N(CH_3)_2]_4$ on Gen-0-3C and Gen-1-3C. For these layers we found $n \approx 0.95-1.59$ on Gen-0-3C and $n \approx 1.15-1.59$ on Gen-1-3C. For N/Ti we found N/Ti of 2.4 (Gen-0-3C) and 1.6 (Gen-1-3C). As with Ta, we find this curious result of the N/M ratio decreasing from Gen-0 to Gen-1. Following arguments similar to that above, both values implicate reactions beyond single ligand exchanges with the terminal $-NH_2$ groups, such as reactions with residual $-OH$ and formation of imido ($-N=Ti$) linkages.[63] Again examination of the binding energy shifts [the Ti(2p) feature in Figure 6a] may prove useful. In this case we find a difference between Gen-0-3C and Gen-1-3C of $+0.73$ eV, implicating, as with Ta, that there is more extensive penetration and reaction of $Ti[N(CH_3)_2]_4$ with residual $-OH$ in the case of the thinner Gen-0-3C layer.

3.3. Discussion. Concerning growth of the dendrons themselves, from our results, two facts are apparent: (i) the thickness (Table 1) and stoichiometry (Table 2) of the layers are in agreement with the expected structure of the layers; and (ii) the efficiency of branching is nearly 100% from the longer 12C anchor, whereas it is clearly less than 100% for the 3C anchor. Why is this so? Steric factors could play some role as the Gen-0-3C layer we form is more dense ($\sim$20%). In addition, the $-NH_2$ in the Gen-0-3C is also more confined to a 2-D plane, as its backbone is short. These two geometric factors could conspire to limit the efficiency of the branching step due to steric repulsion.

A second, and we believe less likely, possibility involves nonideal branching chemistry, for example, self-cyclization, where a single ethylenediame completes the branching step, forming a ring-like moiety. This could also involve a cross-linking reaction with adjacent ester terminations, which are not emanating from the same anchor. These are shown in Scheme 2. In both cases, two [$-C(=O)-NH-$] groups would be formed, but no terminal $-NH_2$ groups, as opposed to the two that should be formed. If these reactions were significant, we would expect that the thickness of the Gen-1 layer would be less than expected for perfect branching (not observed), and its reactivity (initial probability of adsorption) may be also be significantly different from the Gen-0-3C layer (no evidence, see Supporting Information). Also, it is not clear that such reactions would lead to the observed decrease in the contact angle, whereas an increase in the $-NH_2$ density should. Thus, although we cannot completely exclude the occurrence of these

(63) Beaudoin, M.; Scott, S. L. *Organometallics* **2001**, *20*, 237−239.

Scheme 2

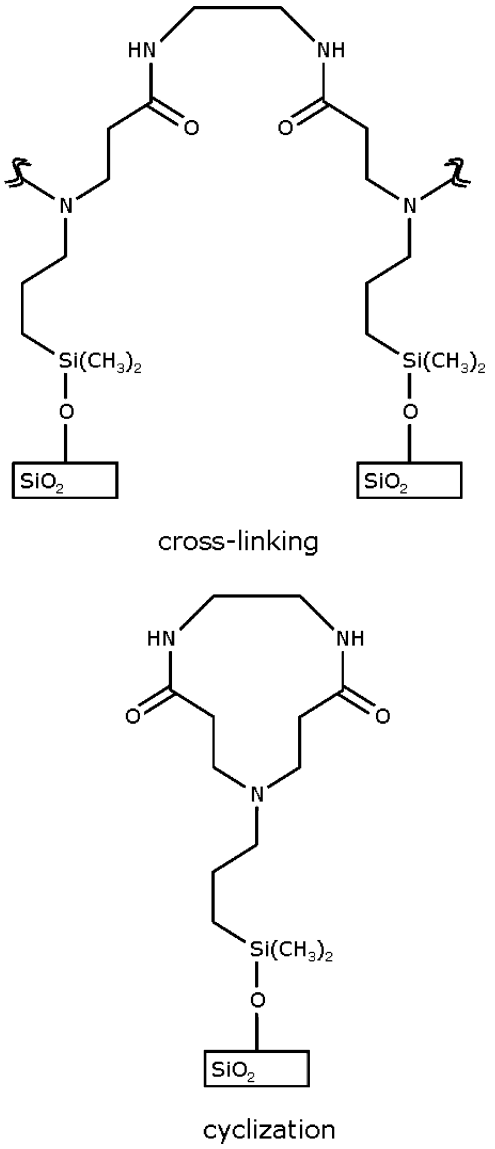

nonideal cyclization/cross-linking reactions, we believe they contribute here little to the observed behavior.

Concerning the reactions with transition metal complexes, we will focus our discussion on the key aspects of the reacted layers: the spatial extent of reaction, their density, and the identity of the species that are formed. Concerning the spatial extent of reaction, these results are summarized above in Table 3. First, concerning the reaction on the Gen-0-3C layer, significant penetration by both the Ta and Ti complex is indicated (from ARXPS) and reaction with residual −OH at the organic/SiO_2 interface is likely (binding energy shifts). For Ta on Gen-0-12C, in contrast, the results indicate that reaction occurs essentially exclusively at the organic/vacuum interface, similar to what we have observed for the reaction of Ti-$[N(CH_3)_2]_4$.[49] For both Gen-1 layers penetration of 40−50% of the organic layer thickness is indicated. For these layers there are additional reactive groups present on the branches, which could provide additional sites for reaction and a driving force for penetration.

As to the density of chemisorbed species, it is clear that in all cases that the chemisorptive capacity of the surface increases

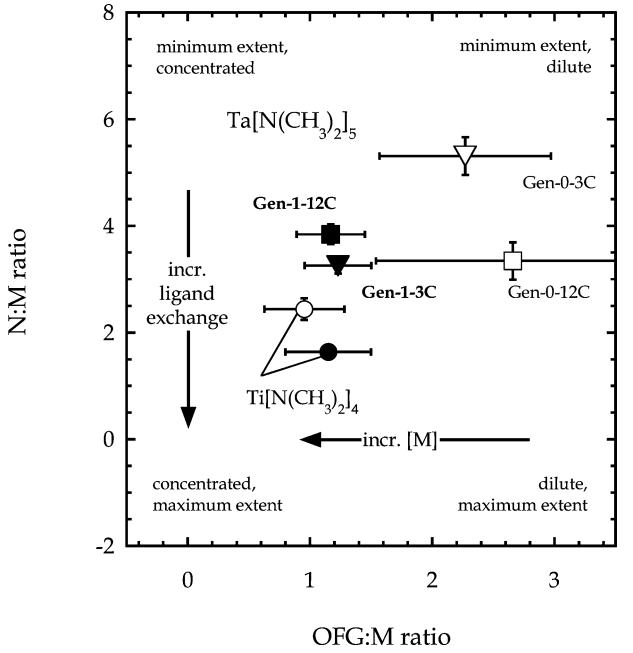

Figure 8. Atomic ratio, N/M, vs the ratio of the OFG (terminal organic functional group, $-NH_2$)/M for saturated adlayers. Open symbols represent results on the Gen-0 layers; filled represent results on the Gen-1 layers. For the ordinate, the density of metal used is that shown in Figure 7 and Table 3 (attenuation corrected).

from Gen-0 to Gen-1, for both anchors and for both metal reactants. In the case of the 3C anchors, these results are somewhat complicated by the likely reactions with residual −OH for the Gen-0-3C layer. The results for the Ta complex shown in Figure 7 suggest a superlinear relationship. One possible reason for a superlinear relationship could be reactions that depend on the square or a higher power of the concentration of reactive end groups. Quantum chemistry calculations[64] indicate that the ligand exchange reactions involving $-R-NH_2$ groups can be catalyzed by the presence of additional groups of this type. Such an effect could contribute to the superlinear dependence.

The identity of the chemisorbed species and the degree of ligand loss appear to depend relatively strongly on the nature of the organic layer, which is indicated by the results shown in Table 4. The amount of ligand loss will depend on the identity of the attacking ligands, their density, and steric issues, including their spatial arrangement. There may also be a relationship between the density of chemisorbed species and the degree of ligand loss, due to interactions between the adsorbed species. In Figure 8 we plot the N/M ratio (*cf.* Table 4) vs the OFG/M ratio (*cf.* Figure 7), and all six combinations of metal complex and organic layer are considered. First, on Gen-0-3C, we can compare the two metal complexes. As already discussed, both complexes likely react via ligand exchange with at least one residual −OH. For $Ta[N(CH_3)_2]_5$, this would produce ≡Si−O−$Ta[N(CH_3)_2]_4$. As the OFG/M ratio is about 2, if these terminal $-NH_2$ groups were merely "spectators" in this case, then N/Ta should be 6. We see that this is close to the case, where possibly there is one additional reaction involving one of these terminal $-NH_2$ groups, leading to a N/Ta of 5. For the reaction of $Ti[N(CH_3)_2]_4$ the situation is quite different. Here

(64) Haran, M.; Engstrom, J. R.; Clancy, P. *J. Am. Chem. Soc.* **2006**, *128*, 836−847.

the density of adsorbed Ti is about twice as much as that of Ta, and the amount of ligand loss is also more, N/Ti = 2.44 ± 0.20. The OFG/M ratio is 0.95 ± 0.33. There are two possibilities that would give this stoichiometry, involving the loss of three ligands, depending on the participation of residual —OH. At this point comparison to previous work[49] is useful, where we found for $Ti[N(CH_3)_2]_4$ on bare chemical oxide (T_s = 30 °C) that N/Ti = 1.22 and the saturation density of Ti was $(5.82 \pm 0.86) \times 10^{14}$ atoms cm^{-2}, or $7.83 \pm 1.20 \times 10^{14}$ atoms cm^{-2} accounting for attenuation effects. The values for $Ti[N(CH_3)_2]_4$ on Gen-0-3C at saturation represent *ca*. 34−42% of these values. Given the coverage of Gen-0-3C of 3.15×10^{14} molecules cm^{-2}, it is plausible that the thin Gen-0-3C layer is primarily occupying/blocking sites. Here the species formed would mostly be $(\equiv Si—O)_3—Ti—N(CH_3)_2$, present in nearly equivalent concentrations to Gen-0-3C. On the other hand, one ligand exchange reaction with Gen-0-3C (in lieu of one with —OH) would give $(\equiv Si—O)_2—Ti—[N(CH_3)_2](NH—R—)$, also consistent with this stoichiometry.

For the Ta complex on Gen-0-12C, as discussed above, the $—R—NH_2$/Ta ratio is 2.7 ± 1.1. The N/Ta ratio is 3.79 ± 0.74, and ARXPS indicates that there is very little penetration of the organic layer, indicating reaction is essentially exclusive with the terminal $—NH_2$ groups. For the sake of argument let us take N/Ta as 4 and OFG/Ta as either 2 or 3. The loss of three ligands and formation of $[(CH_3)_2N]_2Ta(—NH—R—)(=N—R—)$ would satisfy the former, while loss of four ligands and formation of $[(CH_3)_2N]Ta(—NH—R—)_2(=N—R—)$ would satisfy the latter. Further reductions in the N/Ta ratio, or the participation of spectator Gen-0-12C molecules, would require multiple imido linkages, or possible other mechanisms. Interestingly, in earlier work[49] we found for $Ti[N(CH_3)_2]_4$ on Gen-0-12C that OFG/Ti was ∼2 and N/Ti was ∼3 (T_s = 30 °C), implicating an imido species such as $(CH_3)_2N—Ti(—NH—R—)(=N—R—)$.

Finally, we come to the reactions on the Gen-1 layers. Given perfect conversion of Gen-0 to Gen-1, the backbone of the OFG (the branch) is given by $—(CH_2)_2(C=O)NH(CH_2)_2—NH_2$. We present four possible linkages between the backbone and the Ta complex in Scheme 3. On both Gen-1 layers the OFG/Ta stoichiometry is ∼1.2, and N:Ta stoichiometry is 4−5 (Gen-1-12C) and 3−4 (Gen-1-3C). This stoichiometry implies that reaction with a single branch involves the loss of 2−3 ligands and formation of interactions with both the terminal $—NH_2$ and the backbone —NH—(C=O). What is somewhat surprising is that each branch of the structure would be required to react to match the stoichiometry. Apparently, steric interactions between the adsorbed Ta species are not sufficient to limit the reaction. Referring to Scheme 3, two of the linkages (**1b** and **2**) would release two ligands per Ta complex per branch. If multiple linkages can be formed, such as **1b** and **3** (or if **2** forms an imido linkage), this would lead to the loss of three ligands per Ta complex per branch. Of course additional reactions could come into play, including reactions between the adsorbed species themselves to alleviate crowding. For the Ti complex, it appears that considerable loss of ligand has occurred, and N/Ti is ∼ 2. This result would seem to require the participation of residual —OH to entirely strip the Ti complex of its $N(CH_3)_2$ ligands. Given the less than perfect Gen-0 to Gen-1 conversion on the 3C anchor, this is a possibility.

Scheme 3

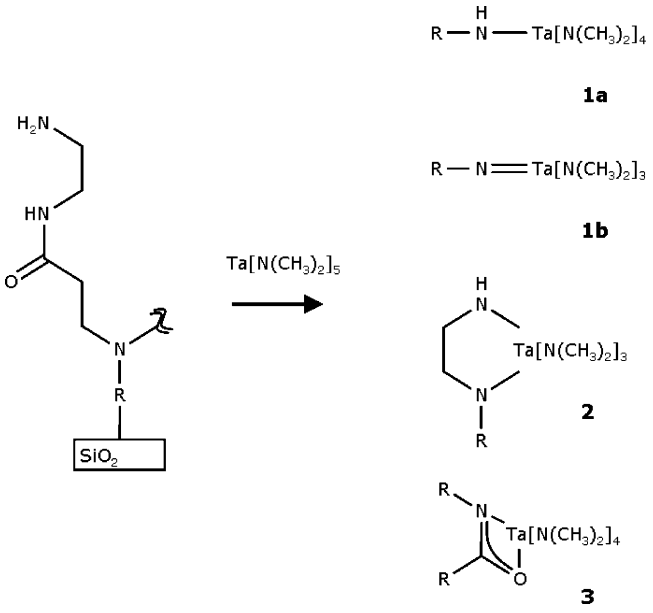

4. Conclusions

We have investigated the growth of branched polyamidoamine dendrons on silicon dioxide and their subsequent reaction with transition metal coordination complexes. From ellipsometry we found that the thicknesses of the layers were in excellent agreement with what one would predict based on realistic molecular models. From XPS, although the stoichiometry of the near surface layers was as expected for a perfect Gen-0 to Gen-1 branching step, it also indicated that the branching step on the shorter anchor perhaps only involved two-thirds of the molecules in the layer, whereas conversion on the longer chain anchor was very efficient. The metal complexes $Ta[N(CH_3)_2]_5$ and $Ti[N(CH_3)_2]_4$ chemisorb on all surfaces examined, exhibiting first-order Langmuirian kinetics. The amount of uptake of the metal (particularly Ta) complexes by the surfaces increases somewhat stronger than linearly with the density of terminal $—NH_2$ groups. Thus, the Gen-0 to Gen-1 step effectively amplifies the reactivity of the surface. For reactions on the thinnest Gen-0-3C layer, penetration of the organic layer occurs and both complexes react with residual —OH at the organic/SiO_2 interface. For the Ta complex on the longer anchor, the reaction is limited to the $—NH_2$ terminal group and involves 3−4 ligand exchange reactions, producing 2−3 amido/imido linkages to the SAM. On the more complicated Gen-1 layers, the reaction of the Ta complex most likely involves the loss of the 2−3 ligands, and each Ta complex appears to interact with on average one of the branches of the dendron, and bonding to both terminal $—NH_2$ and backbone —NH—(C=O)— groups is indicated.

Acknowledgment. This research was supported by the National Science Foundation via the Nanoscale Interdisciplinary Research Team on Inorganic-Organic Interfaces (NSF-ECS-0210693). Additional support was provided by the Semiconductor Research Corporation via the Center for Advanced Interconnect Science and Technology (SRC tasks 1292.003), and an additional grant from the NSF (NSF-ECS-0304483). M.S.

wishes to thank Intel Corporation for a Graduate Fellowship. The authors also wish to thank P. T. Wolczanski for useful discussions.

Supporting Information Available: Details of the experimental procedures including materials used, substrate preparation, synthesis conditions for 3C and 12C Gen-0 and Gen-1 layers, as well as details of the characterization of the organic layers using contact angle measurements, ellipsometry, and XPS. Also available are the details of the analysis of the XPS data, including calculations of the density of the organic layers, data from angle resolved XPS, and uptake curves for the kinetics of adsorption of the metal complexes. This material is available free of charge via the Internet at http://pubs.acs.org.

JA0752944